Available online at www.sciencedirect.com

jmr&t Journal of Materials Research and Technology

journal homepage: www.elsevier.com/locate/jmrt

Short Communication

Experimental evidence for "double-edged sword" effect of the fibrous δ-ferrite on mechanical properties: a case study of Fe-5.95Mn-1.55Si-1.0Al-0.055C medium-Mn steel

Shu Yan [a,b,*], *Tianle Li* [c,**], *Zigan Xu* [d], *Taosha Liang* [e], *Sai Wang* [a,b], *Xianghua Liu* [a,b,f]

[a] *School of Materials Science and Engineering, Northeastern University, Shenyang 110819, China*
[b] *Key Laboratory of Lightweight Structural Materials, Liaoning Province, Northeastern University, Shenyang 110819, China*
[c] *Department of Plasticity Technology, School of Materials Science and Engineering, Shanghai Jiao Tong University, Shanghai 200030, China*
[d] *Steel Institute (IEHK), RWTH Aachen University, Aachen 52072, Aachen, Germany*
[e] *Shenyang National Laboratory for Materials Science, Institute of Metal Research, Chinese Academy of Sciences, Shenyang 110016, China*
[f] *Frontiers Science Center for Industrial Intelligence and Systems Optimization, Northeastern University, Shenyang 110819, China*

ARTICLE INFO

Article history:
Received 3 March 2022
Accepted 14 April 2022
Available online 18 April 2022

Keywords:
Medium-Mn steel
δ-ferrite
Mechanical property
Dislocation

ABSTRACT

An ingenious thermo-mechanical treatment process was utilized on a Fe-5.95Mn-1.55Si-1.0Al-0.055C medium-Mn steel to investigate the effect of fibrous δ-ferrites on mechanical properties. With a large enough cold-rolling reduction ratio (~70%), the morphology of coarsened fibrous δ-ferrites is tailored into homogeneous distributed fragments, which provides a precondition to launch the present study. Direct experimental evidence has been obtained that fibrous δ-ferrites are a double-edged sword for mechanical properties: it improves ductility (by 3.5% ± 1.1%) but decreases tensile strength (by 65 ± 11.5 MPa). This can be related to the accommodation effect of dislocations within coarsened fibrous δ-ferrite grains as soft phase, which decreases the degree of dislocation pile-ups in martensitic matrix, resulting in the limited strengthening effect of dislocations. Additionally, despite significant directionality along rolling direction, the fibrous δ-ferrite grains do not result in anisotropic properties.

* Corresponding author.
** Corresponding author.
E-mail addresses: yanshu_neu@sina.com (S. Yan), ltl26744@163.com (T. Li).

https://doi.org/10.1016/j.jmrt.2022.04.077

1. Introduction

Recently, since medium-Mn steels with 3–12 wt.% Mn are reported to have a high product of strength and elongation (PSE) ranging from 20 to 70 GPa%, the superior combination of strength and ductility makes them to be considered as one of the most promising candidates of advanced high strength steels (AHSS) for automobile lightning [1–6]. Medium-Mn steels usually consist of two phases after the austenite reverted transformation (ART) annealing [7–10], i.e., recrystallized ferrite and reverted austenite. The reverted austenite, which can be provoked to transform into martensite, i.e.,transformation-induced plasticity (TRIP) effect [11,12], is one of the most important reasons for excellent properties through improving work-hardening ability and delaying necking.

To make the manufacture of cold-rolled medium-Mn steels more suitable for modern continuous-annealing process, Suh et al. [13] proposed that Al element was added in medium-Mn steels in order to raise ART annealing temperature and shorten annealing time to 2–3 min. Yet Al as a ferrite stabilizer usually prompts for the residual of δ-ferrite to room temperature [14–16], which can be attributed to no sufficient time to complete the diffusion transformation from δ-ferrite to austenite [17]. Thus, δ-ferrite becomes the third phase in some medium-Mn steels alloyed by Al, especially in low-density medium-Mn steels with high Al content (3.0–7.0 wt.%) [2,17–20]. Not only that, δ-ferrite usually presents coarse and fibrous structure [15], which is quite different from submicron equiaxed grains of the two aforementioned phases. The state-of-the-art knowledge on manipulating the δ-ferrite in medium-Mn steels is limited on the chemistry design level. It is reported that Al and Si facilitate δ-ferrite [2,13,19,22]; on the contrary, C, Mn and Ni suppress δ-ferrite [21–23]. However, research works on tailoring the morphology of the coarsened fibrous δ-ferrite and the effect of δ-ferrite's morphology on mechanical properties of medium-Mn steels has been quite limited.

Thus, in this work, we took the medium-Mn steel containing coarsened fibrous δ-ferrite as the case research object. An ingenious process was designed to manipulate the morphology of δ-ferrite. The relevant mechanical properties are characterized by micro-hardness and tensile tests, and the effect of δ-ferrite morphology on mechanical properties is further discussed. Direct experimental evidence was obtained for the first time in a medium-Mn steel, that coarsened fibrous δ-ferrite grains can be broken into small fragments and the

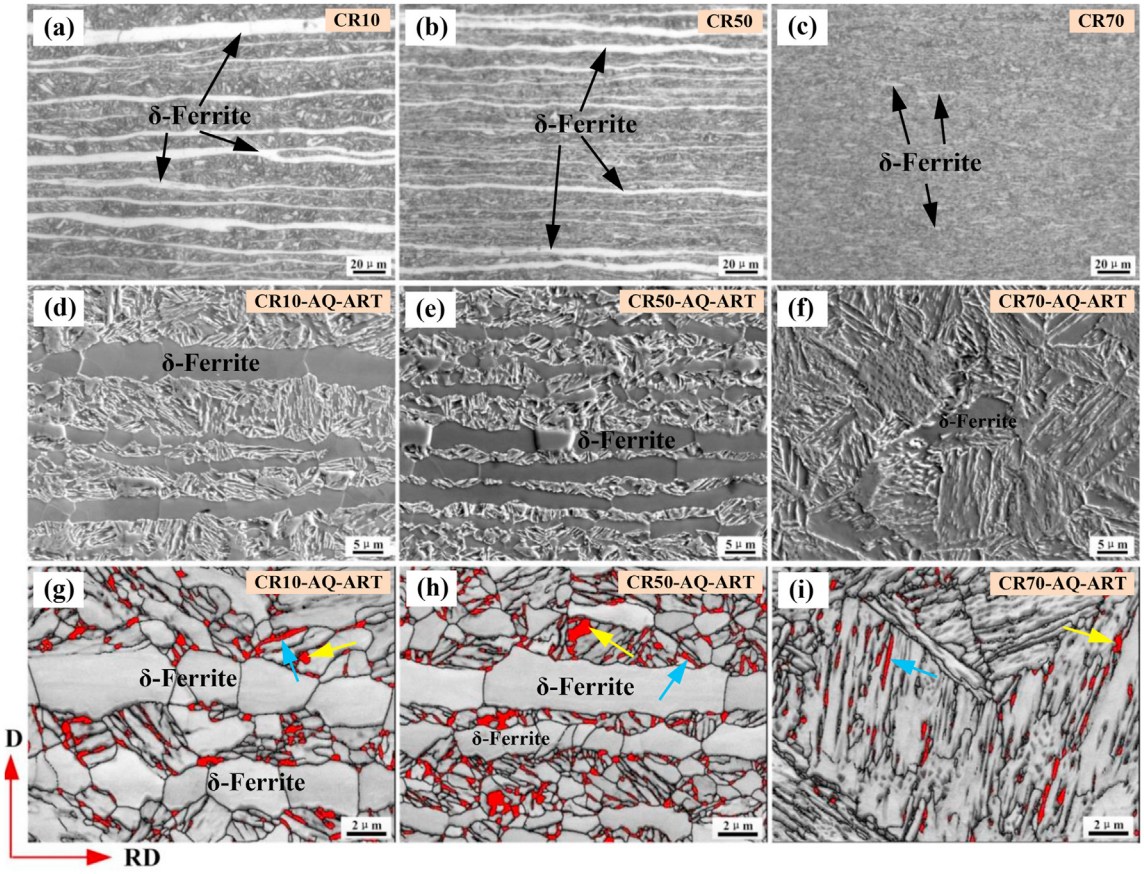

Fig. 1 – Microstructures of the cold-rolled and ART-annealed samples for the investigated steel: OM micrographs of the cold-rolled microstructures with the rolling reduction ratio of 10% (a), 50% (b) and 70% (c); SEM micrographs of the ART-annealed microstructures subjected to the rolling reduction ratio of 10% (d), 50% (e) and 70% (f) before annealing; EBSD characterization of reverted austenite grains (red) overlaid on the ima14ge quality (IQ) maps for the ART-annealed microstructures with the rolling reduction ratio of 10% (g), 50% (h) and 70% (i) before annealing.

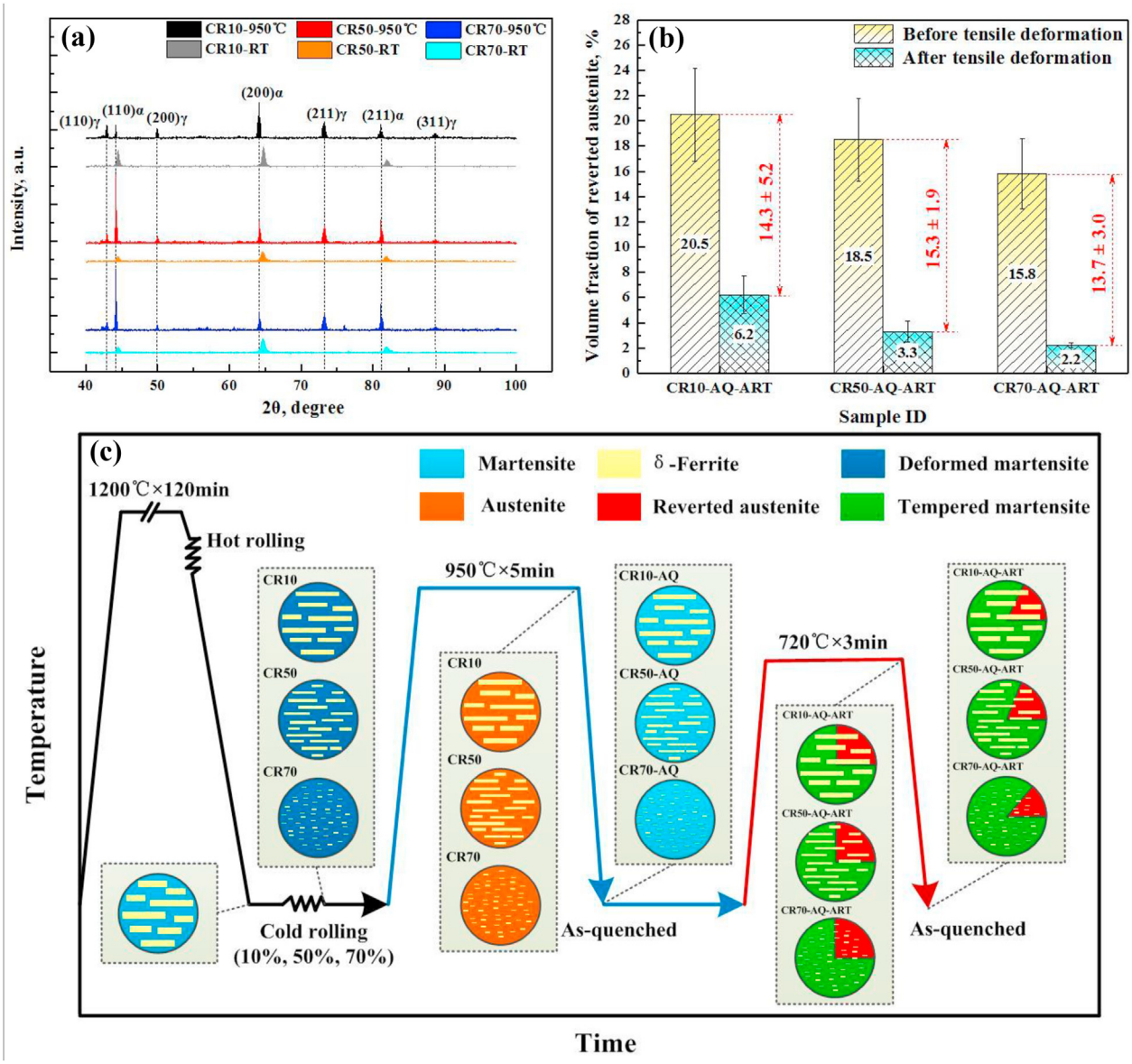

Fig. 2 – (a) In-situ XRD patterns of the cold-rolled samples at room temperature (RT) and 950 °C; (b) The austenite content of the ART-annealed samples before and after tensile deformation based on XRD at RT; (c) The schematic diagram of microstructural evolution through the whole thermo-mechanical process in the present work.

fibrous δ-ferrite is a double-edged sword for mechanical properties. These results can give some references on microstructure design and even alloy composition design for medium-Mn steels in future studies.

2. Experimental procedure

The chemical composition of the present steel is Fe-5.95Mn-1.55Si-1.0Al-0.055C in weight percent. The steel was melted in a vacuum furnace and then forged into a slab with a cross-section dimension of 60 × 100 mm. The slab was hot-rolled into about 4.7 mm in thickness after reheating to 1200 °C for 2 h, and then isothermally held at 600 °C followed by furnace-cooled to room temperature for coiling simulation. The hot-rolled plate was machined into sheets with different target thickness by electric-spark line-cutting, so that these sheets were further cold-rolled into the same thick sheets (about 1.15 mm) under 10%, 50% and 70% rolling reduction ratio. The tensile specimens with a 25 mm gauge length (according to the ASTM-E8 sub-size standard) parallel and vertical to the rolling direction (RD) were machined from the cold-rolled sheets. The former is referred as longitudinal sample (L-sample), and the latter is transverse sample (T-sample). All the samples were austenitized at 950 °C for 5 min and then water-quenched to room temperature. This additional austenitizing-quenching process is necessary in the present work, because if cold-rolled steels with variable rolling reduction ratios are ART-annealed directly, the difference of matrix structure would be significant due to different recrystallization degrees. After that, the ART-annealing at 720 °C for 3 min was carried out for these samples. Based on the process

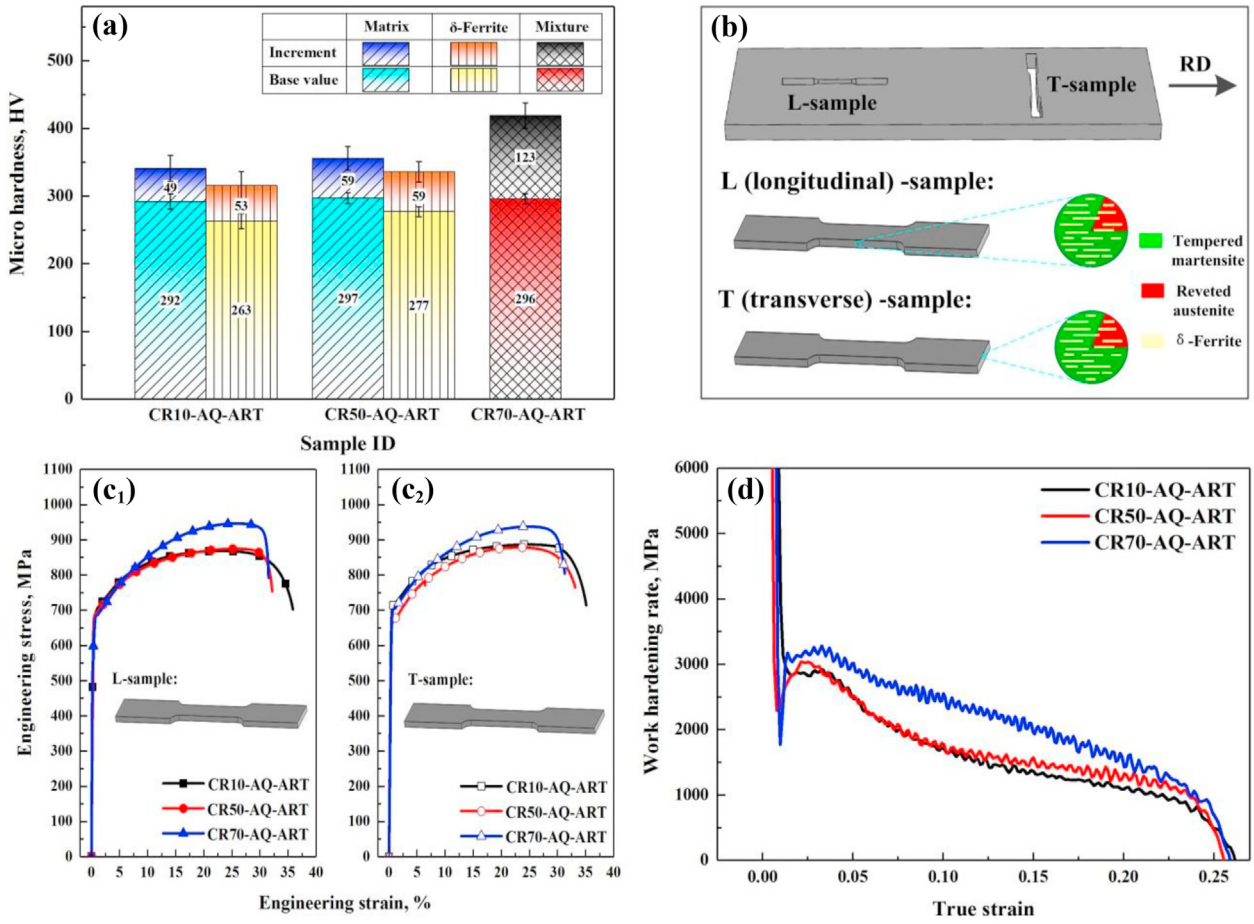

Fig. 3 – (a) The variation of micro-hardness for the samples before and after deformation. The "base value" means the hardness value of ART-annealed sample, and the "increment" indicates the increase of micro-hardness due to tensile deformation. (b) Schematic illustration of directionality of longitudinal and transverse sample on cold-rolled sheet for tensile test. (c_1), (c_2) Engineering stress-strain curves of L-samples and T-samples after ART annealing. (d) Work hardening rate curves of L-samples corresponding to (c_1).

state the sample is in, samples are given IDs for brevity. For example, the CR50 indicates the cold-rolled sample subjected to 50% rolling reduction, and the CR50-AQ-ART means the sample which is successively suffered cold-rolling, austenitizing-quenching and ART-annealing. Quasi-static tensile tests with a strain rate of 2.0×10^{-3} s^{-1} were performed at room temperature (RT). The microstructures were characterized by scanning electron microscopy (SEM), Electron backscatter diffraction (EBSD), transmission electron microscopy (TEM), X-ray diffraction (XRD) at ambient temperature and in-situ XRD at high temperature. The detailed sample preparation methods were in our previous work [24]. The volume fraction of reverted austenite was estimated by the integrated intensities of (200) γ, (220) γ, (311) γ, (200) α, and (211) α peaks.

3. Results and discussion

Fig. 1a-c shows the microstructure of these three cold-rolled samples. Although the thickness of δ-ferrite in the CR50 sample seems to be thinner than that in the CR10 sample due to the increase of reduction ratio, δ-ferrite still presents similar fibrous morphology along the rolling direction as the CR10 sample, as shown in Fig. 1a and b. It is interesting to point out that, when the cold-rolling reduction ratio was further increased to 70%, a quite significant change occurred. These fibrous δ-ferrites were almost broken into small pieces under such a large rolling reduction ratio, as indicated by arrows in Fig. 1c. This provides a favorable condition for the research on the effect of fibrous δ-ferrite on mechanical properties in this medium-Mn steel.

In Fig. 1d-f, SEM micrographs show the final microstructure of these three samples after the whole heat treatment process as mentioned above. δ-ferrites stand out from the matrix of tempered martensite, which can be attributed to the additional austenitizing-quenching process between cold-rolling and ART-annealing. It is worth noting that δ-ferrite remains the same morphology with that in the cold-rolling samples, respectively. Moreover, it is also confirmed that δ-ferrite still existed judging from the diffraction peaks of ferrite when the cold-rolled samples were reheated to 950 °C by in-situ XRD technique, as shown in Fig. 2a. These indicate that δ-ferrite itself did not take part in the transformation of crystalline structure and remained constant fraction

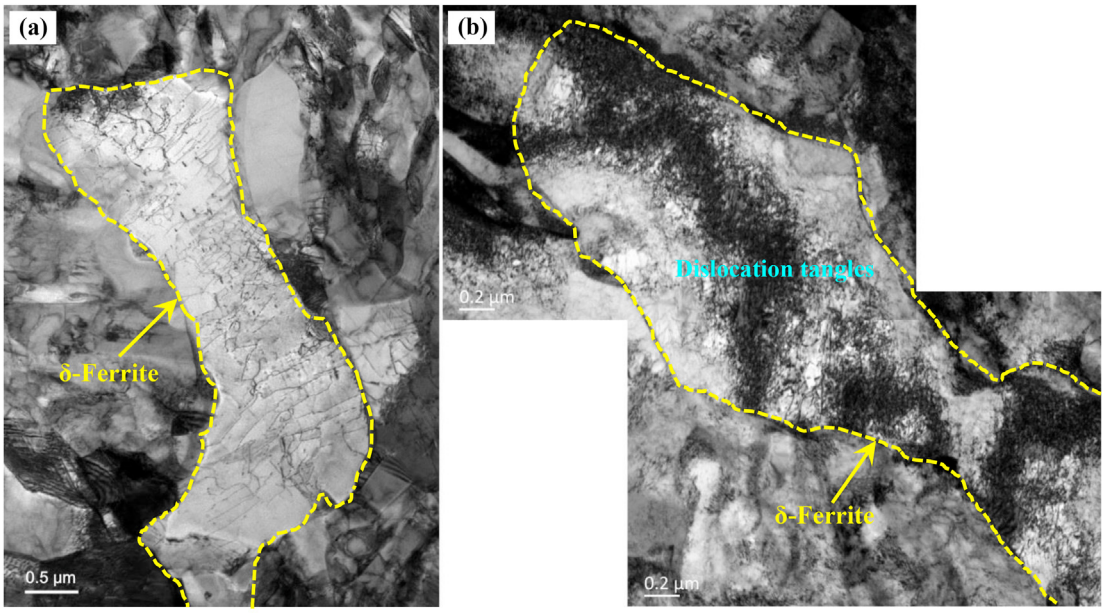

Fig. 4 – TEM micrographs of dislocation substructure within typical δ-ferrite grains before (a) and after (b) tensile deformation for the CR50-AQ-ART sample.

(20.2% ± 3.7% based on statistics) during the whole heat treatment process, though C and Mn elements can be partitioned from δ-ferrite to austenite [14]. In addition to martensitic matrix and δ-ferrite, some reverted austenite grains must be also included in the final microstructures as expected. By XRD examination and analysis at RT, the volume fraction of reverted austenite is respectively quantified as 20.5, 18.5 and 15.8 vol.% for the CR10-AQ-ART, CR50-AQ-ART and CR70-AQ-ART sample, as shown in Fig. 2b. Through EBSD characterization, the reverted austenite grains were observed as shown in Fig. 1g-i. There are two kinds of shapes for reverted austenite grains in each ART-annealed specimen, and the representative blocky and acicular grains are respectively indicated by yellow and blue arrows in Fig. 1g-i.

By now, the microstructural evolution through the heat treatment process designed deliberately has been clarified, which is qualitatively displayed by a schematic diagram in Fig. 2c as well. The most significant difference of the final microstructure among these samples after ART-annealing is the distribution and morphology of δ-ferrite. In the CR10-AQ-ART and CR50-AQ-ART samples, δ-ferrite remains fibrous morphology along the rolling direction, while in the CR70-AQ-ART sample δ-ferrite exists in the form of tiny pieces.

The micro-hardness measurement was utilized to evaluate the hardness difference between matrix and δ-ferrite. Note that the matrix here includes tempered martensite and reverted austenite because it is impossible to distinguish these two phases under the micro-hardness indenter. In the case of ART-annealed samples (before tensile deformation), we refer the measured hardness value as "base value" as shown in Fig. 3a in the present work. As for the CR10-AQ-ART and CR50-AQ-ART sample, the hardness of matrix is comparable, while the hardness of δ-ferrite in CR50-AQ-ART sample is slightly higher than that in CR10-AQ-ART sample. This can be related to the fact that the thickness of fibrous δ-ferrite is thinner and the effect of surrounded martensite on hardness of δ-ferrite is more remarkable in CR50-AQ-ART sample. Notably, in each sample above, the hardness of δ-ferrite is obviously lower compared with that of matrix, thus δ-ferrite is indeed the soft phase [25]. However, for the CR70-AQ-ART sample, due to the fragmentation of δ-ferrite, it is difficult to distinguish the hardness value between matrix and δ-ferrite. Thus, the hardness of mixture phases can only be obtained as shown in Fig. 3a. The measured hardness value of mixture phases in CR70-AQ-ART sample, 296 HV, is also comparable with the hardness of matrix in the CR10-AQ-ART and CR50-AQ-ART samples. Therefore, it can be inferred that there are no significant difference in matrix hardness among these three samples.

Based on the above microstructural characterization and micro-hardness measurement, it can be concluded that the morphology of δ-ferrite is the most significant variable among these three samples. As for the L-sample for tensile test, the long axis of fibrous δ-ferrite is along the direction of force loading during tensile deformation, as displayed in Fig. 3b. From the stress-strain curves in Fig. 3c_1, there is hardly any difference in the yield and tensile strength between the CR10-AQ-ART and CR50-AQ-ART sample, and only the elongation of the latter is slightly lower than the former. Although these two samples show extremely similar microstructure, fibrous δ-ferrite in the CR50-AQ-ART sample is slightly hardened because it is subjected to more severe cold-rolling deformation after all, as shown by micro-hardness values in Fig. 3a. This can be the reason for slightly lower elongation of the CR50-AQ-ART sample. However, the tensile strength of the CR70-AQ-ART sample is approximately 80 MPa higher than the abovementioned two samples; on the contrary, the tensile ductility of the CR70-AQ-ART sample is the worst. Given the remarkable difference of δ-ferrite in the CR70-AQ-ART sample from that in the other two samples, we suggest that fibrous δ-

ferrite as soft phase can play a role in the improvement of ductility but decrease strength to some extent when loading direction is along RD.

The increments of micro-hardness due to tensile deformation were measured and plotted above the base values in Fig. 3a. In either CR10-AQ-ART or CR50-AQ-ART sample, the micro-hardness increments of matrix and δ-ferrite are very close, and the increments between these two samples are also not significantly different. However, for the CR70-AQ-ART sample, the micro-hardness increment of mixture phases is more than twice the increment values of the abovementioned two samples. This indicates that the CR70-AQ-ART sample containing scattered pieces of δ-ferrite has a greater ability to be hardened.

Since the fibrous δ-ferrite as soft phase is significantly directional along RD [14,21,26,27], it is necessary to examine whether the mechanical properties are anisotropic or not. Tensile tests were carried out again using the T-samples so that the loading direction is perpendicular to RD this time. From the stress-strain curves in Fig. 3c_2, the mechanical behaviors of T-samples for these three samples are almost perfectly consistent with L-samples above. This indicates that the directional δ-ferrite grains along RD do not result in anisotropic properties.

Generally, the fibrous δ-ferrite grains after ART-annealing merely contain low-density dislocations as shown in Fig. 4a and have the lower strength. Thus, plastic yielding usually starts from δ-ferrite grains rather than martensitic matrix during tensile deformation [25]. Although this incompatibility of deformation should result in generating geometrically necessary dislocations (GNDs) within fibrous δ-ferrite grains as soft phase at the beginning of deformation for the CR10-AQ-ART and CR50-AQ-ART samples [28], on the larger range of strain, the CR70-AQ-ART sample maintains higher work-hardening rate as shown in Fig. 3d. This is because statistically stored dislocations (SSDs) play decisive roles in hardening at high strain stage. Due to the large grain size (average equivalent diameter of 1.87 ± 1.07 μm according to EBSD detection for the CR10-AQ-ART and CR50-AQ-ART samples) and the priority of deformation, the fibrous δ-ferrite becomes the location in which dislocations (both GNDs and SSDs) accommodate, as shown in Fig. 4b. This decreases the degree of SSD pile-ups in martensitic matrix, resulting in the limited dislocation strengthening contribution. On the contrary, in the absence of the coarse and fibrous δ-ferrite grains, such as the CR70-AQ-ART sample, the accommodation effect of SSDs within δ-ferrite decreases. This promotes the strengthening of matrix, which can be supported by the larger hardness increment due to deformation in the CR70-AQ-ART sample, as displayed in Fig. 3a. This is, of course, the reason that the CR70-AQ-ART sample has higher tensile strength. Dislocation glide within the fibrous δ-ferrite grains gives them a good capacity of plastic deformation, which contributes to relatively higher tensile ductility, just like the CR10-AQ-ART and CR50-AQ-ART samples in the present work. It should be noted that TRIP effect from reverted austenite during deformation also affects the resulting strength and ductility of the present steel. Yet the amounts of reverted austenite which transforms into martensite during deformation were relatively close among these three samples by comparing the austenite content before and after tensile deformation, as shown in Fig. 2b. The contributions of TRIP effect for mechanical properties can be considered identical among these three samples. Therefore, it can be concluded that the fibrous δ-ferrite grains in medium-Mn steels can improve ductility (by 3.5% ± 1.1% for the present steel) but decrease tensile strength (by 65 ± 11.5 MPa for the present steel). This is the effect of double-edged sword of fibrous δ-ferrite for mechanical properties, confirmed by experiments in this work. It is worth pointing out that in some medium-Mn steels with higher carbon content, this double-edged sword effect can be more significant due to the greater difference in strength between δ-ferrite and matrix.

4. Conclusion

In summary, an ingenious thermo-mechanical treatment process was utilized on a Fe-5.95Mn-1.55Si-1.0Al-0.055C medium-Mn steel in this work to investigate the effect of the fibrous δ-ferrite grains on mechanical properties. First of all, the fibrous δ-ferrite grains can be broken into small pieces under a large enough cold-rolling reduction ratio (~70% for this steel), which has been rarely reported in previous studies. This provides a precondition to launch the present study. A designed heat treatment process was carried out to make sure that the morphology of δ-ferrite grains is the only significant difference among the ART-annealed steels subjected to the varied cold-rolling reduction ratios. We found that the fibrous δ-ferrite is a double-edged sword for mechanical properties of the investigated steel. The positive side is that δ-ferrite improves tensile ductility (by 3.5% ± 1.1%), but the negative side is that it decreases tensile strength (by 65 ± 11.5 MPa) in this work. This can be related to the accommodation effect of dislocations within coarsened fibrous δ-ferrite grains as soft phase, which decreases the degree of dislocation pile-ups in martensitic matrix, resulting in the limited dislocation strengthening. In addition, despite the significant directionality along RD, the fibrous δ-ferrite grains do not result in anisotropic properties. We believe that the present study findings can be also extended to other steels containing fibrous δ-ferrite as a reference, such as some medium-Mn steels, low density steels, and even stainless steels etc.

Declaration of Competing Interest

The authors declare that they have no known competing financial interests or personal relationships that could have appeared to influence the work reported in this paper.

Acknowledgements

This study was financially supported by the National Natural Science Foundation of China (No.52174358 and 51704065), the Fundamental Research Funds for the Central Universities of China (No. N2002022) and the 111 Project (B16009).

REFERENCES

[1] Wang MM, Tasan CC, Ponge D, Raabe D. Spectral TRIP enables ductile 1.1GPa martensite. Acta Mater 2016;111:262–72.
[2] Cai ZH, Ding H, Misra RDK, Ying ZY. Austenite stability and deformation behavior in a cold-rolled transformation-induced plasticity steel with medium manganese content. Acta Mater 2015;84:229–36.
[3] Suh D-W, Kim S-J. Scr. Mater. Medium Mn transformation-induced plasticity steels: recent progress and challenges. Scr Mater 2017;126:63–7.
[4] Lee Y-K, Han J. Current opinion in medium manganese steel. Mater Sci Technol 2014;31(7):843–56.
[5] Sun SH, Cai MH, Ding H, Huang HS, Pan HJ. Deformation mechanisms of a novel Mn-based 1GPa TRIP/TWIP assisted lightweight steel with 63% ductility. Mater Sci Eng A 2021;802:140658.
[6] Yan S, Liang TS, Wang ZQ, Yan B, Li TL, Liu XH. Novel 1.4 GPa-strength medium-Mn steel with uncompromised high ductility. Mater Sci Eng A 2020;773:138732.
[7] Wang C, Shi J, Wang CY, Hui WJ, Wang MQ, Dong H, et al. Development of ultrafine lamellar ferrite and austenite duplex structure in 0.2C5Mn Steel during ART-annealing. ISIJ Int 2011;51:651–6.
[8] Arlazarov A, Gouné M, Bouaziz O, Hazotte A, Petitgand G, Barges P. Evolution of microstructure and mechanical properties of medium Mn steels during double annealing. Mater Sci Eng A 2012;542:31–9.
[9] Wan XH, Liu G, Yang ZG, Chen H. Flash annealing yields a strong and ductile medium Mn steel with heterogeneous microstructure. Scr Mater 2021;198:113819.
[10] Wan XH, Liu G, Ding R, Nakada N, Chai YM, Yang ZG, et al. Stabilizing austenite via a core-shell structure in the medium Mn steels. Scr Mater 2019;166:68–72.
[11] Jacques PJ. Transformation-induced plasticity for high strength formable steels. Curr Opin Solid State Mater Sci 2004;8(3–4):259–65.
[12] Jacques PJ, Ladriere J, Delannay F. On the influence of interactions between phases on the mechanical stability of retained austenite in transformation-induced plasticity multiphase steels. Metall Mater Trans A 2002;32. 2759-1768.
[13] Suh D-W, Park S-J, Lee T-H, Oh C-S, Kim S-J. Influence of Al on the microstructural evolution and mechanical behavior of Low-Carbon. Metall Mater Trans A 2010;41(2):397–408.
[14] Aristeidakis JS, Haidemenopoulos GN. Composition and processing design of medium-Mn steels based on CALPHAD, SFE modeling, and genetic optimization. Acta Mater 2020;193:291–310.
[15] Soleimani M, Kalhor A, Mirzadeh H. Transformation-induced plasticity (TRIP) in advanced steels: a review. Mater Sci Eng A 2020;795:140023.
[16] Chen SP, Rana R, Haldar A, Ray RK. Current state of Fe-Mn-Al-C low density steels. Prog Mater Sci 2017;89:345–91.
[17] Yuan Q, Chai LJ, Shen J, Wang H, Guan HT, Guo N, et al. Microstructural characteristics, hardness and wear resistance of a typical ferritic/martensitic steel surface-treated by pulsed laser. Surf Coating Technol 2021;418:127261.
[18] Song H, Yoo J, Kim S-H, Sohn SS, Koo M, Kim NJ, et al. Novel ultra-high-strength Cu-containing medium-Mn duplex lightweight steels. Acta Mater 2017;135:215–25.
[19] Shao C, Hui W, Zhang Y, Zhao X, Weng Y. Microstructure and mechanical properties of hot-rolled medium-Mn steel containing 3% aluminum. Mater Sci Eng A 2017;682:45–53.
[20] Sun B, Fazeli F, Scott C, Brodusch N, Gauvin R, Yue S. The influence of silicon additions on the deformation behavior of austenite-ferrite duplex medium manganese steels. Acta Mater 2018;148:249–62.
[21] Cai ZH, Zhang KM, Jing SY, Ding H. Influence of nickel on microstructure and mechanical properties of medium-manganese steels. Mater Sci Technol 2018;35(1):68–76.
[22] Sun B, Palanisamy D, Ponge B, Gault B, Fazeli F, Scott C, et al. Revealing fracture mechanisms of medium manganese steels with and without delta-ferrite. Acta Mater 2019;164:683–96.
[23] Hu ZP, Xu YB, Zou Y, Misra RDK, Han DT, Chen SQ, et al. Effect of intercritical rolling temperature on microstructure-mechanical property relationship in a medium Mn-TRIP steel containing δ ferrite. Mater Sci Eng A 2018;720:1–10.
[24] Yan S, Liang TS, Chen JQ, Li TL, Liu XH. A novel Cu-Ni added medium Mn steel: precipitation of Cu-rich particles and austenite reversed transformation occurring simultaneously during ART annealing. Mater Sci Eng A 2019;746:73–81.
[25] Song RB, H WF, Zhou NP, Li JJ, Zhang ZR, Wang YJ. Research progress and prospect of Fe–Mn–Al–C medium Mn steels. Chinese J Eng 2020;42(7):814–28.
[26] Cai ZH, Ding H, Misra RDK, Kong H. Unique serrated flow dependence of critical stress in a hot-rolled Fe–Mn–Al–C steel. Scr Mater 2014;71:5–8.
[27] Yan S, Li T, Liang T, Liu X. Adjusting the microstructure evolution, mechanical properties and deformation behaviors of Fe-5.95Mn-1.55Si-1.03Al-0.055C medium Mn steel by cold-rolling reduction ratio. J Mater Res Technol 2020;9(2):1314–24.
[28] Zhu YT, Ameyama K, Anderson PM, Beyerlein IJ, Gao HJ, Kim HS, et al. Heterostructured materials superior properties from hetero zone interaction. Mater Res Lett 2021;9(1):1–31.